Journal of Magnetic Resonance **139,** 139–151 (1999)
Article ID jmre.1999.1751, available online at http://www.idealibrary.com on IDEAL®

Optimization of Offset Frequency in the SORC Pulse Sequence Using Feedback

A. J. Blauch,* J. L. Schiano,* and M. D. Ginsberg†

**Department of Electrical Engineering, The Pennsylvania State University, 227D Electrical Engineering West, University Park, Pennsylvania 16802; and †United States Army Construction Engineering Research Laboratories, P.O. Box 9005, Champaign, Illinois 61826*

E-mail: schiano@steinmetz.ec.psu.edu, m-ginsberg@cecer.army.mil

Received December 18, 1998; revised February 24, 1999

The low signal-to-noise ratio (SNR) of nuclear quadrupolar resonance measurements has motivated research on signal enhancement methods, including multipulse sequences that facilitate signal averaging, the development of interlaced pulse sequences, and super-Q coils. More recently, it has been shown that feedback can be used to automatically optimize pulse sequence parameters, maximizing the SNR. This paper extends this work by using feedback to optimize the offset frequency in the strong off-resonant comb pulse sequence. Analysis and results are presented for a sample of sodium nitrite at both liquid nitrogen and room temperatures. © 1999 Academic Press

Key Words: **nuclear quadrupole resonance; strong off-resonant comb sequence; pulse parameter optimization; feedback control; gradient tuning.**

1. INTRODUCTION

Nuclear quadrupole resonance (NQR) has been investigated as a nonintrusive means for detecting narcotics and explosives (*1–5*). Unlike conventional techniques such as metal detectors, NQR detects the explosive material, not its container. Therefore, NQR enables the detection of minimal metal or completely nonmetallic explosive devices.

The low signal-to-noise ratio (SNR) of NQR measurements presents a challenge in the development of detection systems. Several techniques for improving the SNR have been investigated. Coherent addition of the NQR signals generated by multipulse sequences (*6, 7*) improves the SNR at the expense of increasing the detection time. Interlaced pulse sequences have been developed to lessen the effect of environmental parameters, such as temperature, on the SNR (*8*). NQR detection systems using high-temperature superconducting coils are also being investigated. The SNR increases as the square root of the coil quality factor (Q), even when the bandwidth of the tuned detection circuit is less than the linewidth of the NQR signal (*9*).

A large catalog of multipulse sequences is available for NQR detection experiments. Of particular interest in this paper is the strong off-resonant comb (SORC) sequence (*10*). The SORC sequence has two desirable properties. First, it produces NQR signals whose amplitudes are approximately one-half that of a fully relaxed free induction decay. Second, the SORC NQR signals are generated approximately every T_2^* seconds, thereby providing a large number of signals to be averaged per unit time.

It is well known that the amplitude of the SORC signal is sensitive to pulse parameters (*10, 11*). Suboptimal parameters can decrease the signal intensity by an order of magnitude, negating any improvement in the SNR obtained from the coherent addition of consecutive SORC signals. The optimal parameter values depend on temperature (*12*), distance between the sample and the coil (*1*), and composition of the substance to be detected (*5*).

The sensitivity of the SORC signal to pulse parameters is of particular concern in the development of land mine detection systems. The optimal parameters will vary depending upon the type of land mine, its burial depth, and environmental parameters (*5*). Although a fixed set of pulse parameters can be used to simplify operation of the detection system, this approach yields a suboptimal SNR. A method for automatically optimizing pulse parameters is needed so that the NQR detection system can be used effectively by a nontechnical operator.

Several approaches are available for determining the optimal pulse parameters to maximize the SNR. One technique is to measure the SORC signals for a large set of different parameters, then choose the parameters that yield the highest SNR. This approach is undesirable because it is time consuming. Another technique is to use a feedback system to automatically optimize the pulse parameters. This paper demonstrates such a feedback system and shows that the tuned parameter converges rapidly to its optimal value.

Feedback has already been demonstrated as a means of controlling the state of the nuclear magnetization in NMR (*13*). The pulse width optimization of the SORC pulse sequence using feedback has recently been demonstrated (*14*). It was

1090-7807/99 $30.00

shown that a gradient tuning feedback algorithm can determine the pulse width that maximizes the SORC signal amplitude. This paper demonstrates that a similar algorithm can determine the offset frequency that maximizes the SORC signal energy.

2. MATERIALS AND METHODS

The experiments were performed using a 70-g sample of sodium nitrite, finely ground to avoid the generation of piezoelectric signals (*15*). Another approach for reducing spurious piezoelectric responses, which is well suited to an NQR detection system, is to minimize the electric field produced by the search coil during the application of an RF pulse (*16, 17*). The sample of sodium nitrite was packed into a small vial over which the probe coil was tightly wound. Experiments were performed at both liquid nitrogen (77 K) and room ($\simeq$294 K) temperature. All experiments were conducted at the ν_- transition in ^{14}N.

The transition frequency ν_- is 3.757 MHz at liquid nitrogen temperature and approximately 3.6 MHz at room temperature. When immersed in liquid nitrogen the sample is at a constant temperature, making variations in ν_-, due to temperature, negligible. In contrast, the room temperature experiments subject the sample to variations in ambient temperature as well as heating caused by the probe coil. This is significant because at room temperature the temperature coefficient of the ν_- transition is approximately -1.0 kHz/K (*18*).

The ν_- transition is dominated by a single spin–lattice relaxation time T_{1l} which was measured using the method of progressive saturation. The spin–spin relaxation time T_2 was measured using a two-pulse spin-echo decay. At liquid nitrogen temperature, T_{1l} and T_2 are estimated as 34 s and 6 ms, respectively. At room temperature, they are estimated as 0.3 s and 6 ms, respectively. The T_2^* lineshape parameter was determined from the spin-echo decay. At both liquid nitrogen and room temperatures T_2^* is estimated as 1 ms.

The experiments were performed using a custom-made 1-kW pulsed spectrometer. The system can acquire data, perform calculations, and update pulse parameters in real-time. The Q of the probe coil is approximately 200. To avoid ringing in the receiver following the application of an RF pulse, there is a 240-μs delay between the end of the RF pulse and when the receiver is turned on. The output of the receiver is passed through an eighth-order Butterworth lowpass filter with a cutoff frequency of 10 kHz prior to being sampled at 100 kHz.

3. THE SORC SEQUENCE

The SORC sequence is a periodic series of identical RF pulses with width t_w and period τ. The frequency of the RF pulses is offset Δf Hz above the transition frequency ν_-. The NQR signal observed between the RF pulses reaches a steady-state waveform. The NQR signal induced in the probe coil is mixed with the excitation frequency $\nu_- + \Delta f$, so that the expected frequency of the observed signal is Δf. As an example, Fig. 1 shows experimental data obtained at liquid nitrogen temperature. The data show that the SORC signal is the superposition of two NQR signals, termed Type I and Type II, that are the combination of free induction decays and spin-echoes generated by the pulse sequence. Type I signals immediately follow RF pulses whereas Type II signals immediately precede RF pulses.

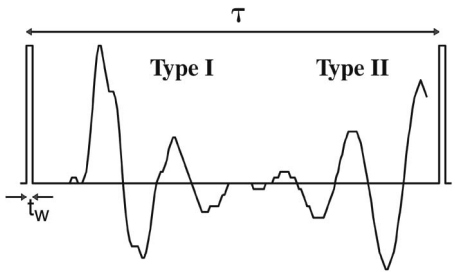

FIG. 1. SORC pulse sequence and filtered SORC signal.

A parametric model that relates the pulse parameters to the SORC signal is needed. Using this model as a guide, a metric is selected to quantify the amplitude of the SORC response. Furthermore, the model aids the development of the control algorithm by providing a means for simulating the response of the closed-loop system. We first identify a model that describes the steady-state relationship between the offset frequency Δf and the SORC amplitude. The transient behavior of the SORC signal due to changes in Δf is considered in Section 4.1.

3.1. Parametric Model

Experimental data indicate that Type I and Type II signals have the form of exponentially decaying sinusoids of the same frequency. It is reasonable to expect that the time constant of the exponential envelopes to be approximately T_2^*. The observed frequency of the SORC signal is sensitive to temperature-induced variations of the NQR transition frequency. As a result, the observed frequency $\overline{\Delta f}$ of the sinusoids may differ from the expected offset frequency Δf. For this reason the observed frequency is expressed as

$$\overline{\Delta f} = \Delta f + \Delta f_e, \qquad [1]$$

where Δf_e is the difference between the observed and expected offset frequencies. Based on these considerations, the Type I and Type II signals are represented as

$$\hat{V}_I(t) = K_I e^{-t/T_2^*} \cos[2\pi(\Delta f + \Delta f_e)t + \theta_I] \qquad [2]$$

$$\hat{V}_{II}(t) = K_{II} e^{-(\tau - t)/T_2^*} \cos[2\pi(\Delta f + \Delta f_e)t + \theta_{II}]. \qquad [3]$$

Accounting for a DC offset V_{DC} at the receiver output, a parametric model of the steady-state SORC signal is

$$\hat{V}(t) = \hat{V}_{I}(t) + \hat{V}_{II}(t) + V_{DC}. \quad [4]$$

Equation [4] is defined in the interval $0 \leq t \leq \tau$, where $t = 0$ corresponds to the center of the RF pulse.

The parameters T_2^*, Δf_e, K_I, K_{II}, θ_I, θ_{II}, and V_{DC} are estimated using observed SORC signals for fixed values of Δf, τ, and t_w. The unknown parameters are estimated using the least-squares method which minimizes (*19*)

$$J(T_2^*, \Delta f_e, K_I, K_{II}, \theta_I, \theta_{II}, V_{DC}) = \sum_{m=L}^{M} [V_f(m) - \hat{V}_f(m)]^2. \quad [5]$$

The observed SORC signal $V(t)$ is passed through an eighth-order Butterworth lowpass filter with a cutoff frequency of 10 kHz. The filtered signal $V_f(t)$ is sampled at $1/T = 100$ kHz to produce the sequence $V_f(m) = V_f(mT)$ of length $M - L + 1$ where $m = L, L + 1, \ldots, M$. Similarly, the estimated sequence $\hat{V}_f(m)$ is obtained by passing the sampled SORC signal estimate $\hat{V}(m)$ through a discrete-time equivalent eighth-order Butterworth lowpass filter. The first $L - 1$ points are not recorded because the receiver is gated off during the ring down time. In order to improve the SNR of the observed SORC signal, 1000 consecutive SORC signals are averaged to produce $V_f(m)$.

As an example, fixing the pulse width and pulse separation at 10 μs and 1 ms, respectively, the parameters T_2^*, Δf_e, K_I, K_{II}, θ_I, θ_{II}, and V_{DC} were estimated for values of Δf ranging from 0 to 3.0 kHz in 100-Hz steps. Experimental data were obtained at liquid nitrogen temperature. For each value of Δf, the SORC signal reached a steady-state waveform within 30 s. One thousand consecutive SORC signals were then acquired and averaged to form $V_f(m)$. In this experiment, $M - L + 1 = 76$ samples of each SORC signal were recorded.

Data obtained for each offset frequency yielded a least-squares estimate of the model parameters. It was found that the estimated values of T_2^*, Δf_e, K_I, K_{II}, θ_I, and V_{DC} did not vary substantially with Δf. For this reason, these parameters were averaged across offset frequencies to obtain $T_2^* = 0.6$ ms, $\Delta f_e = 130$ Hz, $K_I = 0.28$, $K_{II} = 0.27$, $\theta_I = 17°$, and $V_{DC} = -0.11$ V. The estimate of the remaining parameter θ_{II} was observed to be a linear function of Δf. In fact, by replacing Δf in terms of $\overline{\Delta f}$ using [1], we obtained the relationships

$$\theta_{II} = -2\pi\tau\overline{\Delta f} + \theta_I + \pi \quad [6]$$

$$= -2\pi\tau(\Delta f + \Delta f_e) + \theta_I + \pi. \quad [7]$$

TABLE 1

Parameter Estimates for the Parametric SORC Model Based on Data Collected for Offset Frequencies Δf Ranging from 2.1 to 3.0 kHz in 100-Hz Steps

Temperature	K_I [V]	K_{II} [V]	V_{DC} [V]	θ_I [deg]	T_2^* [ms]	Δf_e [Hz]
77 K	0.273	0.261	−0.11	15	0.60	135
294 K	0.077	0.073	−0.11	−32	1.29	−540

Additionally, we observed that these relationships hold independent of the values used for τ and t_w. Based on this observation, the number of unknown parameters in the parametric model can be reduced by replacing θ_{II} with [7] to obtain

$$\hat{V}(t) = K_I e^{-t/T_2^*}\cos[2\pi(\Delta f + \Delta f_e)t + \theta_I] - K_{II}e^{-(\tau-t)/T_2^*} \times \cos[2\pi(\Delta f + \Delta f_e)(t - \tau) + \theta_I] + V_{DC}. \quad [8]$$

In this example, both the pulse separation τ and the pulse width t_w are fixed. If these parameters are changed, then new estimates of K_I, K_{II}, and θ_I are required.

The parametric model [8] reveals the necessary conditions for both constructive and destructive interference between Type I and Type II SORC signals. Kim et al. (*11*) observed that constructive interference between these signals occurs when

$$\tau\overline{\Delta f} = n + \tfrac{1}{2}, \quad n \in \{\ldots, -2, -1, 0, 1, 2, \ldots\}, \quad [9]$$

and that the condition for destructive interference is

$$\tau\overline{\Delta f} = n, \quad n \in \{\ldots, -2, -1, 0, 1, 2, \ldots\}. \quad [10]$$

Referring to [2] and [3], constructive interference occurs when $\theta_I = \theta_{II} + 2\pi n$. Replacing θ_{II} in terms of $\overline{\Delta f}$ using [6] gives [9]. Similarly, destructive interference requires $\theta_I = \theta_{II} + 2\pi n + \pi$ resulting in [10]. It is important to note, for a fixed value of τ, that the minimum difference between offset frequencies resulting in constructive and destructive interference is $1/(2\tau)$.

The ability of the parametric model to predict the SORC response for different values of the offset frequency Δf was experimentally verified at both liquid nitrogen and room temperature using a 10.0-μs pulse width and a 1.0-ms pulse separation. As in the previous experiment, the SORC signal was allowed to reach steady-state, and the subsequent 1000 SORC signals were averaged to produce $V_f(m)$. The average signal was obtained for offset frequencies ranging from 0.0 to 3.0 kHz in 100-Hz steps. A subset of the collected data was

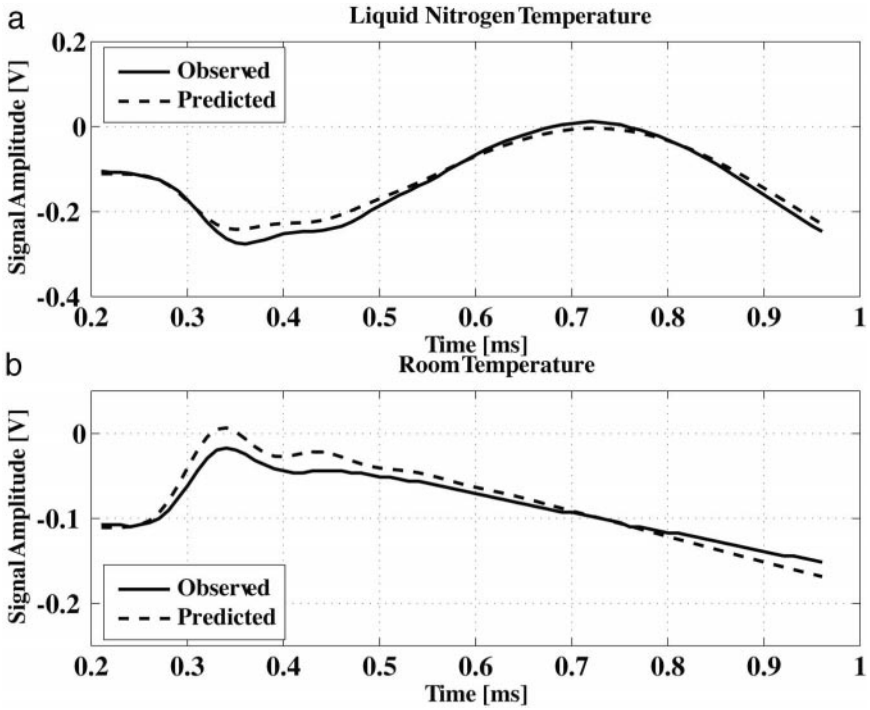

FIG. 2. Comparison of observed and predicted SORC signals for $\Delta f = 1$ kHz at (a) liquid nitrogen and (b) room temperature.

used to estimate the model parameters T_2^*, Δf_e, K_I, K_{II}, θ_I, V_{DC}. These parameters are chosen to minimize

$$J(T_2^*, \Delta f_e, K_I, K_{II}, \theta_I, \theta_{II}, V_{DC}) = \sum_{i=1}^{10} \sum_{m=L}^{M} [V_f(m; \Delta f_i) - \hat{V}_f(m; \Delta f_i)]^2 \quad [11]$$

for a fixed τ and t_w, and offset frequencies $\Delta f_i = 2.0$ kHz + $100i$ ranging from 2.1 to 3.0 kHz (*19*). Table 1 lists the estimated model parameters at both temperatures.

The estimated value of T_2^* is consistent with that obtained from the linewidth of a single spin-echo. In addition, the ratios of K_I at 77 K to K_I at 294 K, and K_{II} at 77 K to K_{II} at 294 K are approximately 3.6. The expected ratios, based on the fact that the magnitude of the NQR signal is inversely proportional to temperature, is 3.8 (*12*).

The estimated parameter values based on data obtained for offset frequencies ranging from 2.1 to 3.0 kHz were used to predict the SORC signals for an offset frequency of 1 kHz at both liquid nitrogen and room temperatures. Figure 2 shows that the observed and predicted SORC signals are in close agreement.

3.2. Signal Metrics

Before developing a feedback algorithm, a measure of the SORC signal intensity must be chosen. The choice of metric can have a significant effect on the performance of the tuning algorithm. As described earlier, the SORC signal is passed through a Butterworth lowpass filter and sampled to produce a sequence $V_f(m)$. Three possible metrics for $V_f(m)$ are considered: peak-to-peak voltage, midsignal amplitude, and signal energy.

The peak-to-peak voltage is defined as

$$V_{pp} = |\max_m\{V_f(m)\} - \min_m\{V_f(m)\}|. \quad [12]$$

The midsignal amplitude

$$V_{mid} = \left| V\left(\frac{M}{2}\right) \right| \quad [13]$$

has also been used as a measure of signal intensity (*10*). The third metric is based on the signal energy (*4*)

$$V_e = \sum_{m=L}^{M} (V_f(m) - V_{DC})^2, \quad [14]$$

where V_{DC} is the DC offset measured at the filter output in the absence of an NQR signal.

In order to determine the sensitivity of each of these metrics to variations in the offset frequency Δf, the metrics were

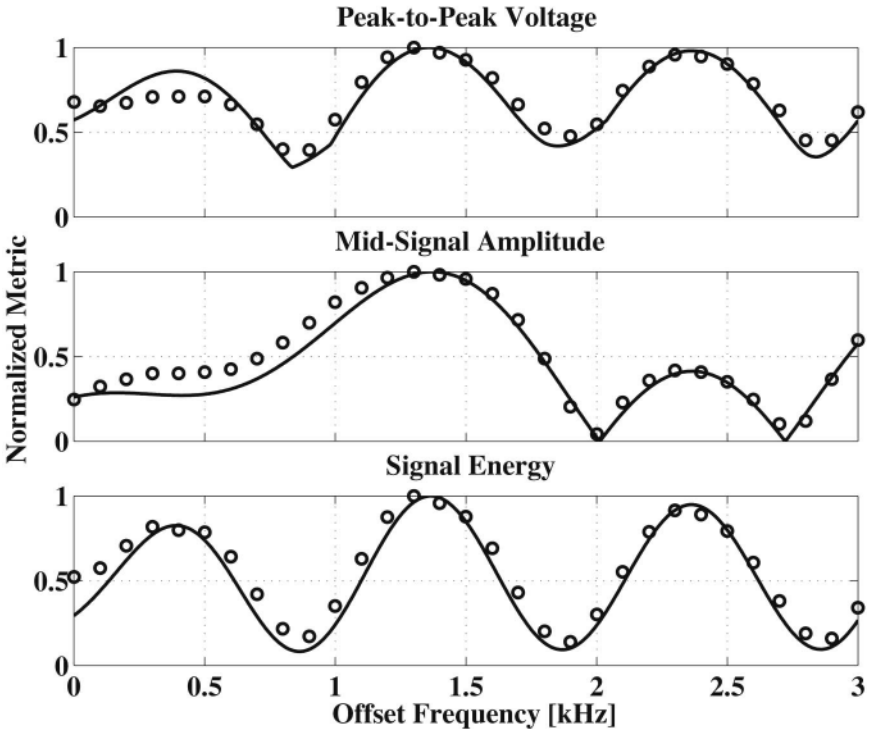

FIG. 3. Normalized metric intensities as a function of offset frequency for a sample of sodium nitrite at 77 K. The open circles show experimental data while the solid curves are obtained using the parametric model.

applied to both experimental data obtained at liquid nitrogen temperature and SORC signals generated using the parametric model in [8]. The experimental data are the same as those used to generate the parameter estimates in Table 1. Figure 3 shows each metric normalized by its maximum value over the range of offset frequencies. The open circles correspond to metric values obtained using experimental data, while the curves correspond to metric values obtained from the parametric model [8] using the parameters in Table 1.

Regardless of the metric used, Fig. 3 shows that the intensity of the experimental data depends on the offset frequency. The cyclic variation with respect to the offset frequency is due to the interference between Type I and Type II signals. Data in Fig. 3 also show that the parametric model accurately predicts the intensity of the SORC signal as a function of offset frequency for each of the three metrics considered. Because the model parameters are estimated using data with offset frequencies ranging from 2.1 to 3.0 kHz, it is significant that the model successfully predicts that the second peak in the signal energy is larger than either the first or third peaks. Furthermore, the location of extrema predicted by [9] and [10] closely match the experimental values for the peak-to-peak voltage and signal energy metrics. Using [9] and the estimated value $\Delta f_e = 135$ Hz, maxima are expected at 0.365, 1.365, and 2.365 kHz. Similarly, Eq. [10] predicts minima at 0.865, 1.865, and 2.865 kHz.

Of the three metrics considered, the energy metric exhibits the largest sensitivity to variations in the offset frequency Δf. In comparison, the midsignal amplitude metric is nearly flat for offset frequencies less than 800 Hz. The extrema of the peak-to-peak voltage metric are not as sharp nor as deep as those for the signal energy metric. Unless otherwise noted, the signal energy metric will be used to quantify the intensity of the SORC signal.

4. FEEDBACK OPTIMIZATION OF OFFSET FREQUENCY

It is well known that the amplitude of the SORC signal depends on the pulse parameters τ, t_w, and Δf (*7, 11*). In an earlier paper it was demonstrated that feedback can automatically determine the optimal pulse width, in the sense of maximizing the SORC signal amplitude, for fixed values of offset frequency and pulse separation (*14*). We now consider the task of choosing the optimal values of offset frequency and pulse separation for a fixed pulse width.

The dependence of the SORC signal intensity on pulse separation for a fixed offset frequency and pulse width is considered first. A set of experiments was performed at liquid nitrogen temperature using a 10-μs pulse width and an offset frequency of 4.0 kHz. The pulse separation was varied from 0.5 to 3.0 ms in 0.025-ms steps. For each pulse separation,

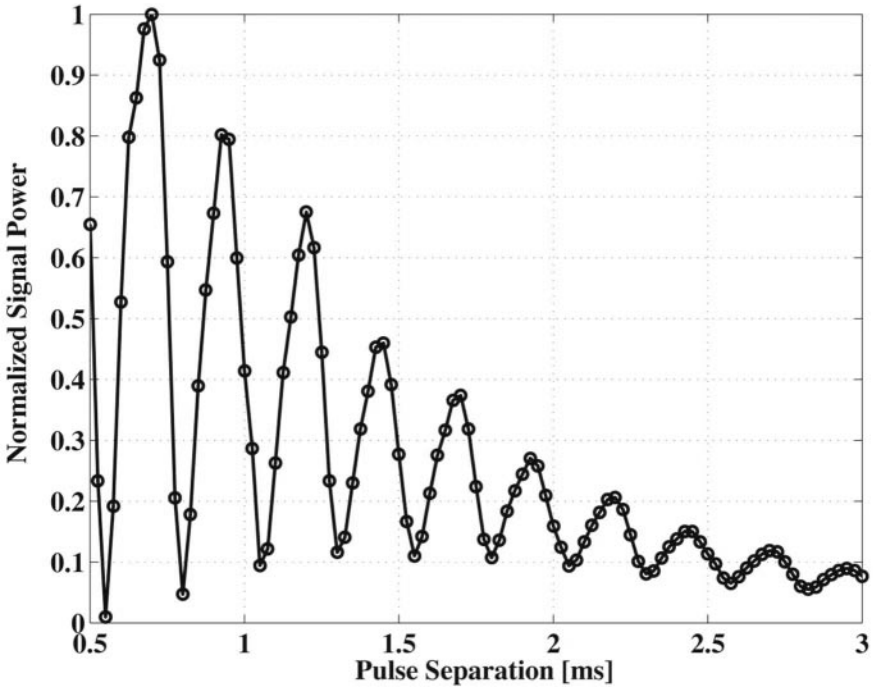

FIG. 4. Normalized signal power as a function of pulse separation; open circles show individual data points.

1000 steady-state SORC signals were filtered and averaged, and the signal energy was calculated as described earlier. Because the data window size is proportional to the pulse separation, it is necessary to compare signal intensity in terms of power instead of energy. The signal power metric is obtained by dividing the signal energy metric for each pulse separation by the corresponding data window size.

Figure 4 shows the normalized signal power as a function of pulse separation. There are two important observations to draw from the data. First, the envelope of the curve increases for smaller values of pulse separation τ. Second, the envelope is modulated by the interference of Type I and Type II signals according to [9] and [10]. The first observation indicates that we should use the smallest value of τ possible. In practice, this value is limited by either the ring down time of the probe coil or the maximum duty cycle of the transmitter. In addition, to avoid a significant loss in signal intensity, it is necessary to choose the offset frequency and pulse separation to satisfy the condition stated in [9] for constructive interference.

Based on these observations, we chose to fix the pulse separation at a small value and automatically tune the offset frequency to maximize the SORC signal intensity. This approach has several advantages. First, in addition to increasing the signal intensity, a small value of pulse separation also increases the number of SORC signals available for averaging per unit time. Second, fixing the pulse separation provides a constant window size for comparison of signal energies. Third, by fixing τ, the time required to obtain a single averaged SORC signal is not dependent upon the parameter which is being optimized. Fourth, Fig. 4 shows that the amplitude of the local maxima varies greatly with pulse separation. In contrast, Fig. 3 shows that the amplitude of local maxima of signal energy does not vary significantly with offset frequency. This fact simplifies the design of the control algorithm, which must only find a local maxima when varying the offset frequency.

In order to design a feedback algorithm that optimizes the offset frequency, the transient response of the SORC signal intensity to variations in the offset frequency must be known. So far we have only considered a parametric model that relates the steady-state signal intensity to changes in offset frequency. The dynamics of the SORC pulse sequence have been addressed earlier (*20–22*). However, a closed-form expression relating the transient response to changes in the pulse parameters is not available. The next section uses experimental data to characterize the transient behavior of the SORC signal.

4.1. Transient Response

Two experiments were performed to observe the transient response of the SORC signal energy. The first experiment reveals the transient response at the start of the SORC sequence for a fixed offset frequency of 2.50 kHz, while the second experiment shows the transient response caused by a step change in the offset frequency from 2.55 to 2.50 kHz. Experiments were performed at room and liquid nitrogen temperatures, with the pulse width t_w and pulse separation τ fixed at 20.0 μs and 1.0 ms, respectively.

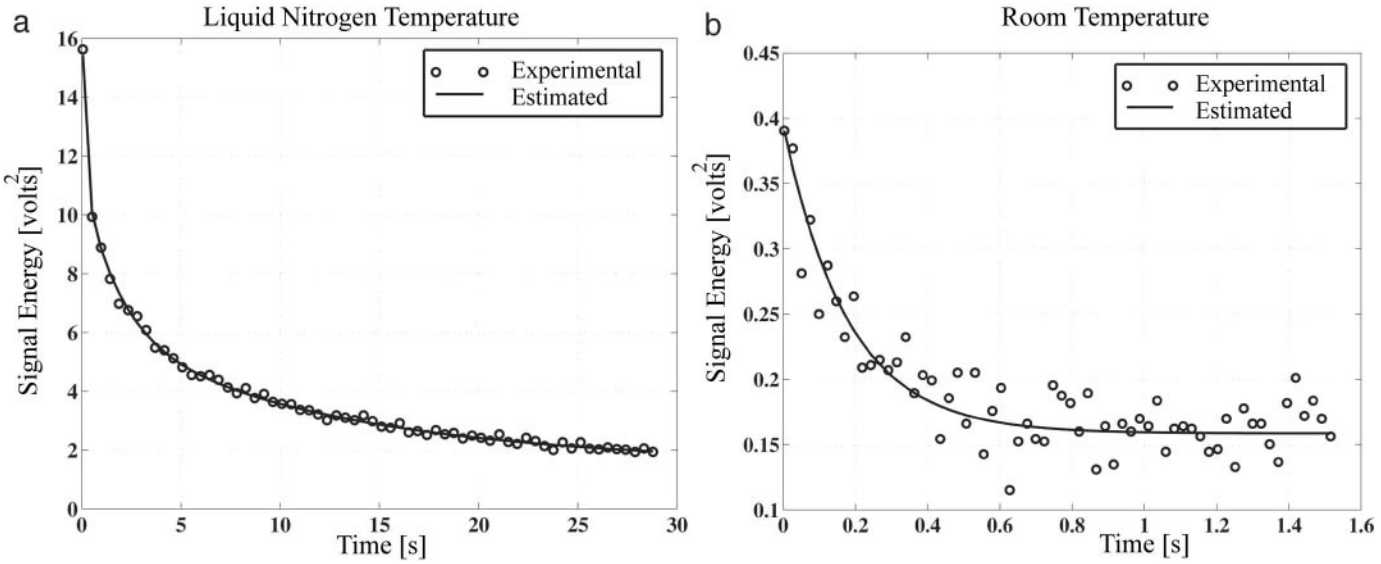

FIG. 5. Transient response of signal energy for an offset frequency of 2.50 kHz.

Individual SORC signals are indexed by the integer n, where $n = 0$ corresponds to the SORC signal following the first RF pulse. In the first experiment, Δf is fixed at 2.50 kHz and the SORC signals are recorded starting from $n = 0$ until the SORC signal energy reaches a steady-state value.

In the second experiment, the offset frequency is fixed at 2.55 kHz for the first N_d RF pulses. The number of delay pulses N_d is chosen so that the SORC signal energy reaches a steady-state value during the time interval $N_d\tau$. Starting with the N_dth RF pulse, the offset frequency is fixed at 2.50 kHz. In this experiment, SORC signals are recorded for $n \geq N_d$.

The open circles in Fig. 5 show the signal energy of each measured SORC signal in the first experiment as a function of time $t = n\tau$, where τ is the fixed pulse separation. The data obtained at both temperatures suggest an overdamped transient response in signal energy

$$\hat{V}_e(n\tau) = A_0 + A_1 e^{-n\tau/\tau_1} + A_2 e^{-n\tau/\tau_2} + \cdots, \qquad [15]$$

where $\hat{V}_e(n\tau)$ is an estimate of the observed signal energy of the nth SORC signal, τ_i are time constants, and A_i are amplitudes. The time constants τ_i describe the rate at which the signal energy metric, and hence SORC waveform, approach steady-state. In contrast, the time constant in the parametric model describes the shape of the steady-state SORC waveform. The parameters τ_i and A_i are chosen to minimize

$$J(\tau_i, A_i) = \sum_n [V_e(n\tau) - \hat{V}_e(n\tau; \tau_i, A_i)]^2, \qquad [16]$$

where $V_e(n\tau)$ is the energy of the nth measured SORC signal. The solid curves in Fig. 5 show the estimated signal energy $\hat{V}_e(n\tau)$ obtained using the time constants in Table 2. At liquid nitrogen temperature, more than one time constant is present. In contrast, at room temperature, only one time constant is observed. At both temperatures, the dominant time constant is about one-half the spin–lattice relaxation time T_{1l}.

Next we consider the transient response of the SORC signal to a change in offset frequency. The open circles in Fig. 6 show the signal energy of the measured SORC signals versus $t = (n - N_d)\tau$, where the offset frequency is stepped from 2.55 to 2.5 kHz at $t = 0$. As in the previous experiment, the data were fit to an exponential curve using the least-squares method. The estimated signal energy $\hat{V}_e(n\tau)$ based on the time constants in Table 2 is indicated by the solid curves in Fig. 6. Note that two time constants were required to describe the observed relaxation for data obtained at liquid nitrogen temperature. In contrast, only one time constant was required when the sample was at room temperature.

Data for both experiments show that the SORC signal energy reaches a steady-state value within approximately T_{1l} s. This observation is consistent with previous results (*14*). In terms of the control design, if the feedback algorithm updates

TABLE 2
Estimated Time Constants Observed in the Transient Response of the SORC Signal Energy

Temperature	Experiment	Time constants (s)		
Liquid nitrogen	1	12.5	1.91	0.18
	2	7.73	0.20	—
Room	1	0.180	—	—
	2	0.177	—	—

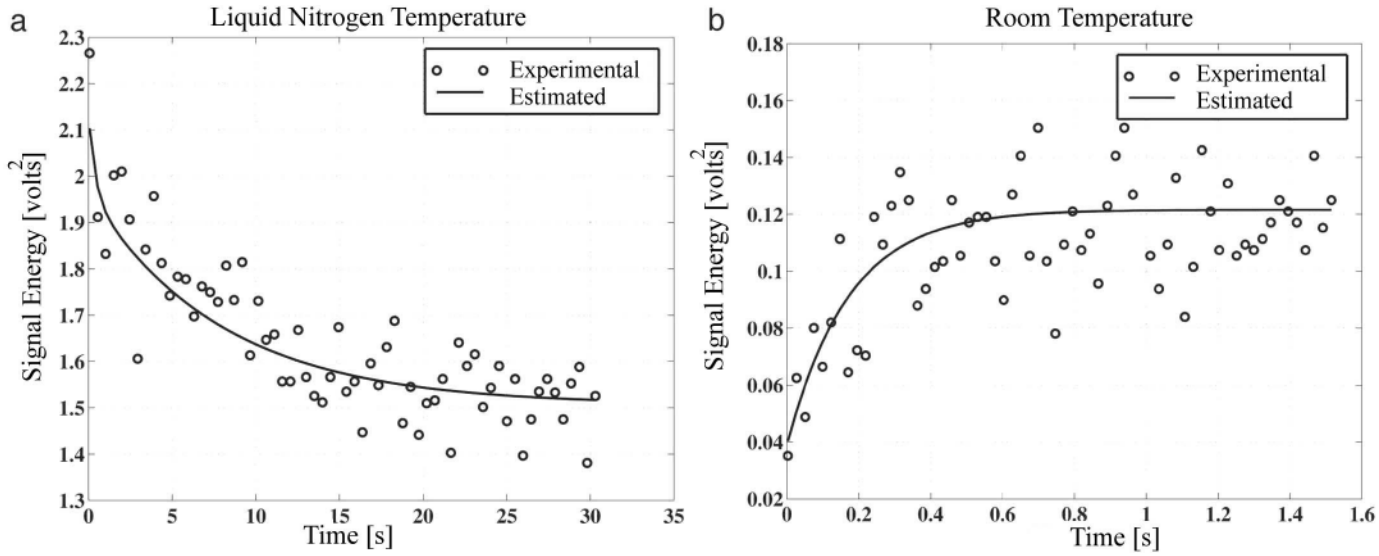

FIG. 6. Transient response of the signal energy for a step change in offset frequency from 2.55 to 2.5 kHz.

the offset frequency on the order of T_{1l}, these results indicate that the algorithm must take into account the dynamic behavior of the system. On the other hand, if the feedback algorithm varies the offset frequency on a time scale larger than T_{1l}, the task of choosing Δf simplifies to a static optimization problem.

4.2. Gradient Algorithm

The selection of an algorithm that automatically adjusts the offset frequency Δf is guided by several considerations. Because a closed-form dynamic model relating changes in the offset frequency to variations in the SORC signal energy is unavailable, the algorithm cannot be model dependent. The algorithm should not be computationally intensive so that it can be implemented in real-time. Finally, the algorithm should have a minimal number of free design parameters to reduce its sensitivity to variations in operating parameters. For example, in land mine detection applications, the exact temperature, position of the mine with respect to the probe coil, and the electrical properties of the soil separating the probe coil and mine are not known a priori.

In light of these considerations, a gradient tuning algorithm based on the steepest ascent method is used to optimize the offset frequency. Figure 7 shows the modified SORC sequence used to implement the gradient algorithm. The pulse separation τ and pulse width t_w are fixed across the entire sequence. The integer k indexes segments of the pulse sequence that use a fixed offset frequency $\Delta f(k)$. At the start of the kth segment, the first N_d SORC signals are not recorded. During the interval $N_d\tau$, the energy of successive SORC signals approach a steady-state value. The subsequent N_a SORC signals are filtered, sampled, and averaged. The energy of the averaged SORC signal is denoted as $V_e(k)$. The interval during the remaining N_c SORC signals represents the computational delay required to determine the offset frequency $\Delta f(k+1)$ for the $(k+1)$th segment of the pulse sequence.

The optimization objective is to choose the offset frequency $\Delta f(k)$ that maximizes the performance index

$$J(\Delta f(k)) = J(k) = V_e(k).$$

The optimal offset frequency is found using the method of

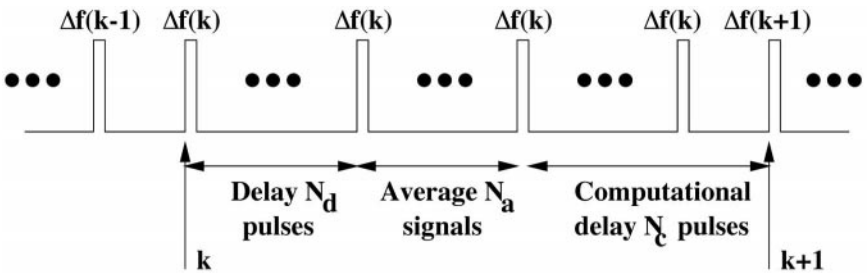

FIG. 7. SORC pulse sequence for gradient tuning algorithm experiments.

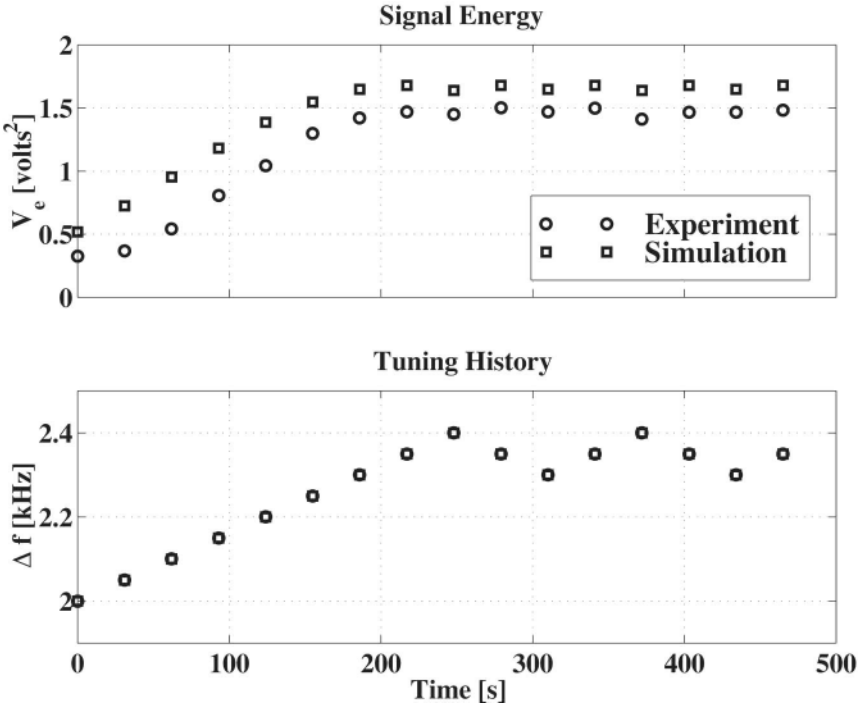

FIG. 8. Response of the closed-loop system at liquid nitrogen temperature for an initial offset frequency of 2.0 kHz and a delay time of $N_d\tau = 30$ s. Experimental data and simulation results are shown by circles and squares, respectively.

steepest ascent which is an iterative approach (*19*). The offset frequency is updated as

$$\Delta f(k+1) = \Delta f(k) + \lambda \nabla_{\Delta f} J(k), \qquad [17]$$

where λ is a positive learning factor and $\nabla_{\Delta f} J(k)$ is the gradient of the performance index with respect to the offset frequency Δf. The gradient $\nabla_{\Delta f} J(k)$ represents the ratio of the change in signal energy to the change in offset frequency. This gradient can be approximated as

$$\nabla_{\Delta f} J(k) = \frac{J(k) - J(k-1)}{\Delta f(k) - \Delta f(k-1)}. \qquad [18]$$

To reduce the sensitivity of the gradient to noise, especially when the change in offset frequency is small, the gradient $\nabla_{\Delta f} J(k)$ is replaced with

$$\nabla_{\Delta f} J(k) = G(J(k) - J(k-1)) G(\Delta f(k) - \Delta f(k-1)), \qquad [19]$$

where the function $G(x)$ is defined as

$$G(x) = \begin{cases} 1 & x \geq 0 \\ -1 & x < 0. \end{cases} \qquad [20]$$

The function $G(x)$ is similar but not equal to the function $\text{sign}(x)$. For $x = 0$ the function $G(x)$ is equal to one while $\text{sign}(x)$ is equal to zero. This definition is necessary to ensure that the gradient approximation is bounded. Using the approximation in [19], the gradient $\nabla_{\Delta f} J(k)$ can only take values of $+1$ or -1. As a result, the learning factor λ in [17] represents the step-size by which the offset frequency is changed. Because the gradient never vanishes, $\Delta f(k)$ can only converge to the optimal value in a limit cycle whose radius is equal to the step-size λ.

The choice of the step size λ is important. If the step size is too large, the offset frequency $\Delta f(k)$ may not converge. On the other hand, if the step size is too small, $\Delta f(k)$ will converge slowly. Earlier we pointed out that the minimum distance between offset frequencies corresponding to constructive and destructive interference is $1/(2\tau)$. This observation places an upper bound on the step-size. Through trial and error, it was found that the step-size of $\lambda = 0.1/(2\tau)$ allows the algorithm to locate the optimal offset frequency within approximately 10 iterations.

When the number of delay pulses N_d is sufficiently large so that the SORC signal energy reaches a steady-state value before data is acquired, the parametric model can be used to simulate the response of the closed-loop system. Simulation data are presented along with experimental results in the next section.

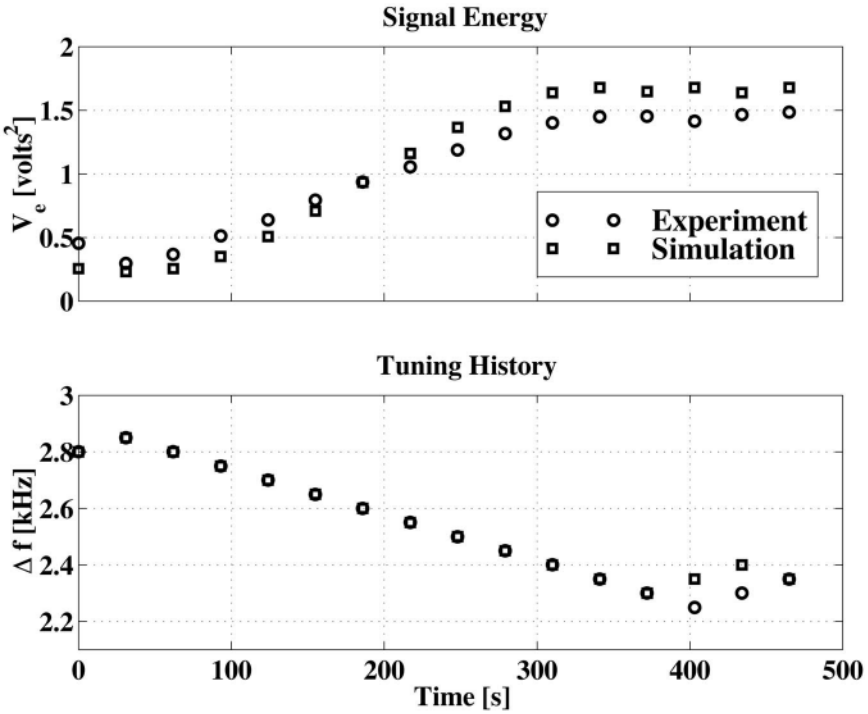

FIG. 9. Response of the closed-loop system at liquid nitrogen temperature for an initial offset frequency of 2.8 kHz and a delay time of $N_d\tau = 30$ s. Experimental data and simulation results are shown by circles and squares, respectively.

4.3. Experimental Results

The ability of the gradient algorithm to maximize the signal energy by adjusting the offset frequency was assessed in a series of experiments. In each experiment, the parameters $\tau =$ 1 ms, $t_w = 20.0$ μs, $N_a = 1000$, $N_c = 2$, and $\lambda = 0.1/(2\tau) =$ 50 Hz were fixed. The initial offset frequency $\Delta f(0)$ and the number of pulses N_d over which the SORC signal is allowed to reach steady-state were varied. The experiments show the effect of different values of N_d and the initial offset frequency $\Delta f(0)$ on the performance of the gradient algorithm.

The first two experiments were performed at liquid nitrogen temperature. The estimated value of Δf_e is approximately equal to the value shown in Table 1. Choosing the delay time $N_d\tau =$ 30 s was sufficient to allow the SORC signal energy to reach a steady-state value before data were acquired.

In the first experiment the initial offset frequency $\Delta f(0)$ is set to 2.0 kHz. Figure 8 shows experimental results along with computer simulations of the closed-loop system generated using the parametric model. The upper plot in Fig. 8 shows the signal energy V_e while the the lower plot shows the tuning history of the offset frequency Δf. Both V_e and Δf are plotted as a function of time. The time between adjacent data points is $(N_d + N_a + N_c)\tau = 31$ s. The experimental and simulation data are shown by open circles and squares, respectively. The second experiment is identical to the first, except that the initial offset frequency is set to 2.8 kHz. Figure 9 shows the experimental data and simulation results.

Figures 8 and 9 show that the gradient algorithm tuned the offset frequency to about 2.3 kHz, in both simulation and experiment. This is consistent with the result expected from [9]. Using $\tau = 1$ ms and taking into account the estimate $\Delta f_e =$ 135 Hz, constructive interference is expected at offset frequencies $\Delta f = 0.365$, 1.365, and 2.365 kHz. The algorithm tuned both initial offset frequencies to the closest value of Δf yielding constructive interference.

The third experiment is performed at liquid nitrogen temperature with $N_d\tau = 2$ s, which is more than an order of magnitude less than T_{1l}. Experimental results obtained for initial offset frequencies of 2.0 and 2.8 kHz are shown in Fig. 10. Note that the tuned offset frequency oscillates about its initial value, while SORC signal energy decays toward zero. This failure is expected because the gradient ascent algorithm does not take into account the dynamics of the SORC sequence. By reducing $N_d\tau$ to a value much smaller than T_{1l}, the SORC signal energy does not reach a steady-state value before data acquisition occurs. Similarly, the parametric model is based on the steady-state SORC response, and so it cannot be used to accurately simulate the behavior of the closed-loop system.

The final experiment is conducted at room temperature using a delay time $N_d\tau = 1.5$ s which is about five times T_{1l}. The experimental response of the gradient tuning algorithm is shown in Fig. 11 for an initial offset frequency of 2 kHz. Within six iterations that span 15 s, the gradient algorithm tuned the offset frequency to maximize the SORC signal energy.

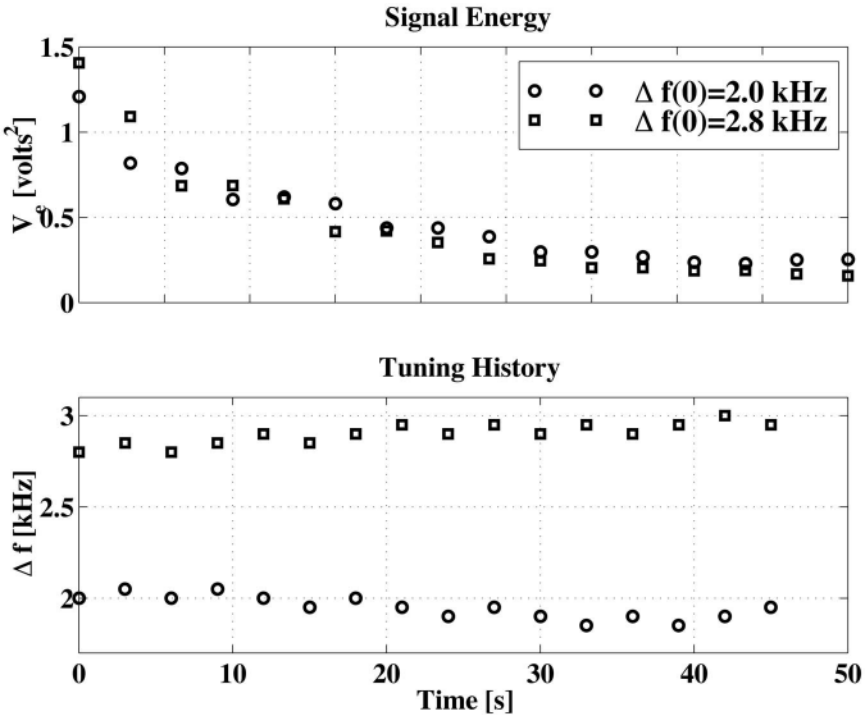

FIG. 10. Response of the closed-loop system at liquid nitrogen temperature for initial offset frequencies of 2.0 and 2.8 kHz, and a delay time of $N_d\tau = 2$ s.

5. DISCUSSION

The ability to automatically optimize pulse parameters is important when NQR is used in detection instrumentation operated by nontechnical individuals. We have shown that feedback control provides a means for maximizing signal energy through automatic adjustment of offset frequency in the

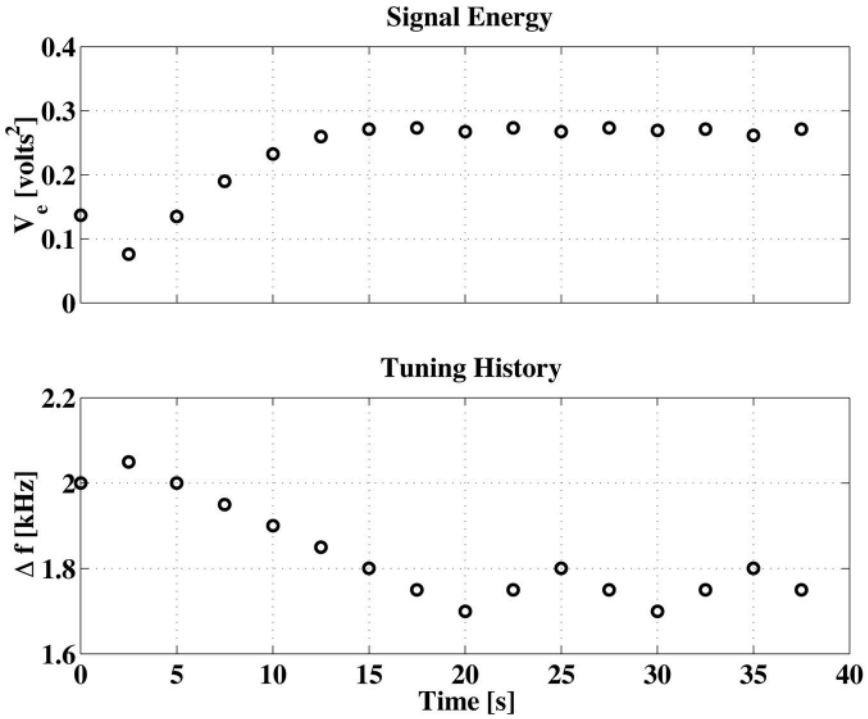

FIG. 11. Response of the closed-loop system at room temperature for an initial offset frequency of 2.0 kHz and a delay time of $N_d\tau = 1.5$ s.

SORC pulse sequence. In order to understand how the offset frequency affects the steady-state SORC signal, and to enable simulation of the gradient tuning algorithm, a parametric model that relates the offset frequency to the steady-state SORC signal was identified. The parametric model in [8] accurately predicts the constructive and destructive interference patterns of the SORC pulse sequence as the offset frequency Δf is varied. The offset frequencies that result in extrema located by [9] and [10] are consistent with previously reported experimental results (*10*). When used to compute the signal metrics considered in this paper, the parametric model results were nearly identical to experimental values.

Regardless of the method used to adjust Δf to maximize the SORC response, a metric of the SORC signal intensity is needed. Both simulation results and experimental data indicate that, of the three metrics considered, the signal energy is the most sensitive to variations in offset frequency Δf.

There are many approaches for choosing the offset frequency that maximizes the SORC signal energy. For example, one could use an FFT of the average SORC waveform to determine the actual offset frequency. However, for a 1-ms pulse spacing the frequency resolution of an FFT is 1 kHz. On the other hand, the gradient tuning algorithm is able to locate the optimal offset frequency to within ± 50 Hz. The parametric model was successful in simulating the gradient tuning algorithm as long as the delay time $N_d\tau$ was sufficiently large to allow the signal energy to reach a steady-state value.

This paper demonstrated that a gradient tuning algorithm can successfully optimize the offset frequency in the SORC sequence. This gradient algorithm has only one free design parameter, the learning factor λ. However, by setting $\lambda = 0.1/(2\tau)$, the offset frequency approached an optimal value within 10 iterations. This design parameter is chosen independent of the sample temperature, T_{1l}, T_2, T_2^*, and t_w.

The insensitivity of the algorithm to variations in sample temperature is important because the NQR resonant frequencies are strongly dependent on temperature (*23*). As an example, in sodium nitrite, the temperature coefficient is approximately -1 kHz/K (*18*). Not surprisingly, the value of Δf_e was found to vary by at least 500 Hz in room temperature experiments where the sample temperature was unregulated. Despite the large variations in Δf_e, the gradient tuning algorithm successfully located the optimal offset frequencies.

The gradient algorithm requires that the delay time $N_d\tau$ be approximately T_{1l} or larger so that the SORC signal energy reaches a steady-state value before it is used to update the offset frequency. When this condition is violated, the tuned offset frequency no longer converges and the signal energy is not maximized. At room temperature, where $T_{1l} = 0.3$ s, the delay time $N_d\tau$ is smaller than the time $N_a\tau$ used for averaging, and so the required delay does not impose a significant time penalty.

Combining these results and those obtained by (*14*), an autocalibration algorithm can be developed that optimizes both the pulse width and the offset frequency to obtain the maximum signal energy. Although it is possible to apply both optimization methods back to back, we are currently investigating algorithms that simultaneously tune both pulse width and offset frequency.

The results presented in this paper were obtained using a material that provides a single, narrow NQR line and serves as a proof of concept for an autocalibration algorithm. In the case of explosives, there are multiple, wide lines. For example, in RDX there are 6 transition frequencies. The lines are separated by a minimum of 48 kHz with a maximum linewidth of 460 Hz (*4*). In this case there is still sufficient separation between the resonance frequencies to allow the excitation of a single transition. Therefore, we expect the optimization algorithm presented in this paper to be applicable to RDX. On the other hand, in TNT there are 12 resonance lines corresponding to six distinct nitrogen sites (*2*). Because the separation between adjacent lines is only several kilohertz, the tuning algorithm would require modifications if multiple lines are excited.

6. CONCLUSION

This paper presented a parametric model that accurately predicts the steady-state SORC waveform as the offset frequency Δf is varied. A gradient tuning algorithm that automatically adjusts the offset frequency to maximize the SORC signal energy was demonstrated. The gradient tuning algorithm method affords several advantages. It allows a nontechnical operator to automatically calibrate an NQR detection system. The algorithm does not require a detailed dynamic model, and is therefore insensitive to variations in the dominant time constants of the NQR signal response. In addition, because the algorithm is not computationally intensive, it can be implemented in real-time.

ACKNOWLEDGMENTS

This work is funded in part by the United States Army Construction Engineering Research Laboratories under Contract DACA 88-95-K-0002.

REFERENCES

1. T. Hirschfeld and S. M. Klainer, Short range remote NQR measurements, *J. Mol. Struct.* **58,** 63–77 (1980).
2. R. A. Marino, Nuclear quadrupole resonance spectroscopy, *in* "Chemistry and Physics of Energetic Materials," pp. 715–738, Kluwer Academic, Norwell, MA (1990). NATO ASI series. Series C, Mathematical and physical sciences, v. 309.
3. J. P. Yesinowski, M. L. Buess, A. N. Garroway, M. Ziegeweid, and A. Pines, Detection of ^{14}N and ^{35}Cl in cocaine base and hydrochloride using NQR, NMR, and SQUID, *Anal. Chem.* **67**(13), 2256–2263 (1995).
4. T. N. Rudakov, V. T. Mikhaltsevich, and O. P. Selchikhin, The use of multi-pulse nuclear quadrupole resonance techniques for the detection of explosives containing RDX, *J. Phys. D Appl. Phys.* **30**(9), 1377–1382 (1997).

5. V. S. Grechishkin and N. Ya Sinyavskii, New technologies: Nuclear quadrupole resonance as an explosive and narcotic detection technique, *Phys. Uspekhi,* **40**(4), 393–406 (1997).
6. R. A. Marino and S. M. Klainer, Multiple spin echoes in pure quadrupole resonance, *J. Chem. Phys.* **67**(7), 3388–3389 (1977).
7. M. L. Buess, A. N. Garroway, and J. B. Miller, NQR detection using a meanderline surface coil, *J. Magn. Reson.* **92,** 348–362 (1991).
8. J. A. S. Smith and J. D. Shaw, Method of and apparatus for NQR testing selected nuclei with reduced dependence on a given environmental parameter. United States Patent Number 5583437, December 1996.
9. B. H. Suits, A. N. Garroway, and J. B. Miller, Super-Q detection of transient magnetic resonance signals, *J. Magn. Reson.* **132,** 54–64 (1998).
10. R. A. Marino, S. M. Klainer, and T. B. Hirschfeld, Fourier transform nuclear quadrupole resonance spectroscopy, *in* "Fourier, Hadamard, and Hilbert Transforms in Chemistry," pp. 147–182, Plenum Press, New York (1982).
11. S. S. Kim, J. R. P. Jayakody, and R. A. Marino, Experimental investigations of the strong off-resonant comb (SORC) pulse sequence in ^{14}N NQR, *Z. Naturforsch. A J. Phys. Sci.* **47A,** 415–420 (1992).
12. T. P. Das and E. L. Hahn, Nuclear quadrupole resonance spectroscopy, *in* "Solid State Physics," Suppl. 1, Academic Press, New York (1958).
13. J. L. Schiano, R. L. Magin, and S. M. Wright, Feedback control of the nuclear magnetization state: Modeling and control design. *IEEE Trans. Med. Imaging,* **MI-10**(2), 138–147 (1991).
14. J. L. Schiano, T. Routhier, A. J. Blauch, and M. D. Ginsberg, Feedback optimization of pulse width in the SORC sequence. *J. Magn. Reson.,* submitted.
15. E. Rodrigues and M. M. Rodrigues, Piezoelectric effects in nuclear-quadrupole resonance, *J. Chem. Phys.* **44,** 2200–2201 (1965).
16. L. Pandey and D. G. Hughes, Electrostatic shield for the suppression of piezoelectric ringing in pulsed NMR. *J. Magn. Reson.* **56,** 443–447 (1984).
17. D. G. Hughes and L. Pandey. Spurious signals caused by the piezoelectric ringing of $NaNO_2$ in pulsed NMR. *J. Magn. Reson.* **56,** 428–442 (1984).
18. T. Oja, R. A. Marino, and P. J. Bray, ^{14}N nuclear quadrupole resonance in the ferroelectric phase of sodium nitrite. *Phys. Lett.* **26A**(1), 11–12 (1967).
19. D. G. Luenberger, "Linear and Nonlinear Programming," 2nd ed., Addison-Wesley, Reading, MA (1984).
20. R. S. Cantor and J. S. Waugh, Pulsed spin locking in pure nuclear quadrupole resonance, *J. Chem. Phys.* **73**(3), 1054–1063 (1980).
21. G. E. Karnaukh, B. B. Provotorov, and A. K. Khitrin. Thermodynamic theory of multipulse NQR experiments. *Soviet Phys. J. Exp. Theor. Phys.* **57**(1), 93–96 (1983).
22. D. Ya. Osokin, V. L. Ermakov, R. H. Kurbanov, and V. A. Shagalov. The quasistationary states in multipulse NQR. *Z. Naturforsch. A J. Phys. Sci.* **47A,** 439–445 (1992).
23. T. Kushida, G. B. Benedek, and N. Bloembergen, Dependence of the pure quadrupole resonance frequency on pressure and temperature. *Phys. Rev.* **104**(5), 1364–1377 (1956).